PROCEEDINGS A

royalsocietypublishing.org/journal/rspa

Research

Cite this article: de Oliveira PM, Mesquita LCC, Gkantonas S, Giusti A, Mastorakos E. 2021 Evolution of spray and aerosol from respiratory releases: theoretical estimates for insight on viral transmission. *Proc. R. Soc. A* **477**: 20200584.
https://doi.org/10.1098/rspa.2020.0584

Received: 22 July 2020
Accepted: 14 December 2020

Subject Areas:
biomedical engineering, fluid mechanics

Keywords:
respiratory releases, viral transmission, COVID-19

Author for correspondence:
P. M. de Oliveira
e-mail: pm580@cam.ac.uk

Evolution of spray and aerosol from respiratory releases: theoretical estimates for insight on viral transmission

P. M. de Oliveira[1], L. C. C. Mesquita[1], S. Gkantonas[1], A. Giusti[2] and E. Mastorakos[1]

[1]Hopkinson Laboratory, Department of Engineering, University of Cambridge, Cambridge, UK
[2]Department of Mechanical Engineering, Imperial College London, London, UK

PMdO, 0000-0002-5527-8128; LCCM, 0000-0001-5086-696X; SG, 0000-0002-5354-578X; AG, 0000-0001-5406-4569; EM, 0000-0001-8245-5188

By modelling the evaporation and settling of droplets emitted during respiratory releases and using previous measurements of droplet size distributions and SARS-CoV-2 viral load, estimates of the evolution of the liquid mass and the number of viral copies suspended were performed as a function of time from the release. The settling times of a droplet cloud and its suspended viral dose are significantly affected by the droplet composition. The aerosol (defined as droplets smaller than 5 μm) resulting from 30 s of continued speech has O(1 h) settling time and a viable viral dose an order-of-magnitude higher than in a short cough. The time-of-flight to reach 2 m is only a few seconds resulting in a viral dose above the minimum required for infection, implying that physical distancing in the absence of ventilation is not sufficient to provide safety for long exposure times. The suspended aerosol emitted by continuous speaking for 1 h in a poorly ventilated room gives 0.1–11% infection risk for initial viral loads of 10^8–10^{10} copies ml_l^{-1}, respectively, decreasing to 0.03–3% for 10 air changes per hour by ventilation. The present results provide quantitative estimates useful for the development of physical distancing and ventilation controls.

THE ROYAL SOCIETY PUBLISHING

1. Introduction

As the scientific debate on the droplet-related mechanisms allowing for the global spread of the SARS-CoV-2 virus evolves, attention has been shifting from *droplet* transmission towards *aerosol* as a possible additional route of transmission [1]. Illness caused by the inhalation of small-sized virus-laden droplets that can remain in the air long after being emitted by an infected (symptomatic or asymptomatic) individual, seems to explain a number of known outbreaks where safety measures put in place by local authorities were adopted, but contagion still occurred [2]. Due to the limited information on how respiratory droplet clouds evaporate while settling by gravity, the values and decay rates of the suspended viral dose emitted in respiratory releases are yet unknown. As a result, a great deal of uncertainty might be associated with current modelling practices used to define emergency control policies to minimize the damage caused by the COVID-19 disease as it develops. This work sheds light on the droplet-versus-aerosol debate by providing a theoretical characterization of the time evolution of droplets from the moment of their emission, bridging these estimates to our current knowledge of the SARS-CoV-2 characteristics [3–7] in order to provide a metric of viral dose levels and decay.

Although significant efforts were made to investigate the time scales associated with single respiratory droplets undergoing the combined action of evaporation and gravity (starting from [8] and refined more recently by Xie *et al*. [9]), only recently a full experimental account of the actual range of droplet sizes produced in a respiratory release was possible. Due to fast atomization processes happening at the mouth, vocal chords, and lungs, during breathing, speaking, or coughing, a wide range of droplets from sub-micrometre to millimetre size are emitted, requiring various experimental techniques combined to account for such wide-ranging sizes [10–12]. In addition to previous efforts, evidence that the evaporation process of a sputum droplet might be significantly affected by the droplet composition was shown very recently in experiments [13] and evaluated for a 10-μm diameter droplet [14]. As a multi-component droplet evaporates, the concentration of non-volatile components increases, affecting evaporation rates and ultimately dictating the final 'equilibrium' diameter reached by the droplet.[1] Hence, the final droplet diameters found in [13,14] were between 20–40% of the initial value, approximately, depending on the assumed concentration of protein modelled in the droplet. Such large variation leads to considerable errors in the modelling of *airborne* transmission, which assumes the resulting droplet nuclei to lie within the aerosol class, that is, typically below 5 μm [15].[2] Additionally, the decomposition of the saliva/mucus can add further uncertainty to the problem. Changes in droplet physico-chemical characteristics during evaporation, for example, as the increase in concentration of salts and surfactants, and the effects of water reabsorption on the stability of the SARS-CoV-2 virus are unknown. Such effects could also impact the short-range, short-time scale problem of *droplet* transmission.

From a fluid mechanics perspective, it is useful to define the droplets emitted in a respiratory release as (i) those that always follow the motion of air flows, that is, *small droplets*, and (ii) those that exhibit a mainly ballistic-type of behaviour, that is, *large droplets* [8]. The cut-off diameter between small and large droplets is understood to vary between 60 and 120 μm, affected by droplet composition and ambient conditions [9] as well as local flow phenomena related to the exhaled gas puff [17,18] and ventilation streams [18]. Although the Stokes number of a particle or droplet (i.e. the ratio of its characteristic time scale to the flow time scale) is generally used to evaluate how these move in relation to air flows (for $\mathrm{St} \ll 1$, droplets are expected to closely follow the flow [19]), an arbitrary size of 5–10 μm is often used to define *aerosol* particles which are

[1]Mass-transfer equilibrium is achieved in a multi-component evaporating droplet as the vapour pressure exerted by the water at the droplet's interface is approximately that of the water vapour in ambient air.

[2]Airborne transmission is typically defined by the health community as contagion through virus-laden droplet nuclei (i.e. 'dry' sputum particles) by a susceptible person [15]. From an aerosol science or fluid mechanics perspective, the term *droplet nucleus* evokes the possibility of hygroscopic growth, that is, water absorption by the particle leading to the formation of a water droplet. This mechanism might, in fact, occur in a sputum-derived droplet nucleus as it undergoes changes in humidity as, for example, while being inhaled [16].

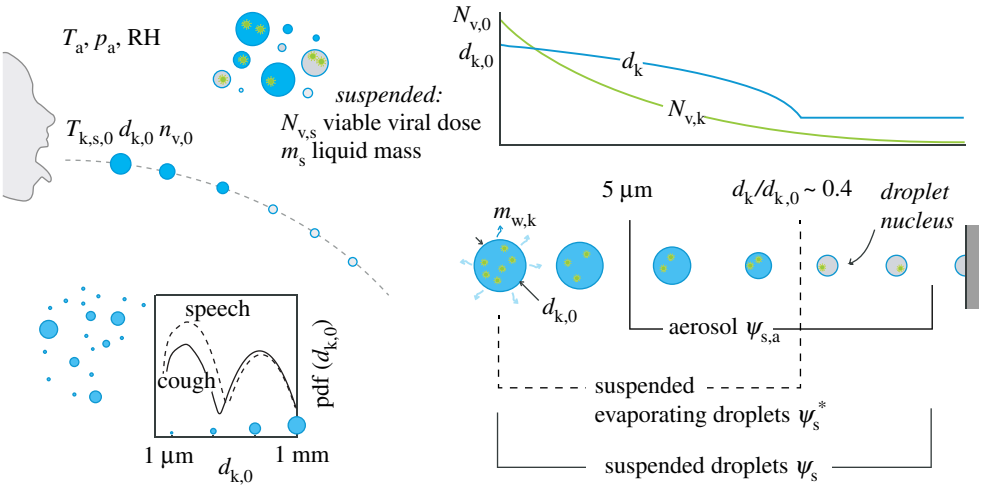

Figure 1. Illustration of the problem and main parameters. (Online version in colour.)

then used for ventilation calculations. Recent findings suggest that higher values of around 20 µm should be used instead [18,20]. In general, it is not quite proper to assume a predefined cut-off value, because the droplet size below which the droplet cloud fully follows the flow and remains in the air depends on the flow itself, due to the upwards or downwards ventilation currents and the turbulence levels.

Here, an evaluation of the evaporation and settling of droplet clouds emitted in respiratory releases is carried out, providing information on the time between the short-time scale problem of droplet transmission up to the long-time scale problem of aerosol transmission. State-of-the-art models are used for the prediction of evaporation and to account for droplet size distribution and concentration in two modes of droplet exhalation: by coughing and speaking. In this paper, we:

— Evaluate the size distribution and life-time of the suspended droplet cloud and the effects of ambient conditions on these quantities.
— Provide ensemble averages of mass and droplet number concentration in terms of their initial values at the emission source.
— Investigate, in the previously mentioned analyses, the evolution of different classes of droplets representing specific viral transmission scenarios: the whole of the suspended droplet cloud; only droplets within the aerosol category; and each of these two groups excluding 'dry' droplet nuclei.
— Evaluate the emitted viral dose from sick individuals through coughing and speaking, and investigate the evolution of the suspended viable viral dose.

To demonstrate the impact of such metrics for physical distancing/ventilation, three canonical problems are considered: uniform flow from the emitter to the receptor, jet decay simulating the short-range flow pattern from the emission, and the well-mixed room focusing on the long timescales of the aerosol and on the risk of infection.

2. Models and methods

(a) Droplet motion and evaporation

The sputum droplets are assumed to be spherical particles. The trajectory of the centre of mass is computed using the so called 'Lagrangian' approach where the equations of motion (balance of

momentum) are solved for each particle independently (figure 1). Both the gravity and buoyancy forces are considered together with the aerodynamic drag. All the other forces, such as Basset, Magnus and Saffman forces, as well as virtual mass are neglected [21]. The governing equations in a Lagrangian specification that describe the motion of the k-th droplet are as follows:

$$\frac{\mathrm{d}\mathbf{X}_k}{\mathrm{d}t} = \mathbf{v}_k \tag{2.1}$$

and

$$\frac{\mathrm{d}\mathbf{v}_k}{\mathrm{d}t} = \frac{3C_{D,k}}{d_k}\left(\frac{\rho_\mathrm{g}}{\rho_\mathrm{l}}\right)|\mathbf{u}-\mathbf{v}_k|\,(\mathbf{u}-\mathbf{v}_k) + \left(1-\frac{\rho_\mathrm{g}}{\rho_\mathrm{l}}\right)\mathbf{g} \tag{2.2}$$

where t indicates the time, $\mathbf{g}$ is the acceleration of gravity, d_k is the diameter of the droplet, $\mathbf{X}_k$ and $\mathbf{v}_k$ are the position and velocity vectors of the droplet, $\mathbf{u}$ is the velocity vector of the gas, ρ is the density, and the subscripts g and l refer to the gas and liquid phase, respectively. The parameter $C_{D,k}$ in the aerodynamic drag term of equation (2.2) is a function of the Reynolds number of the droplet Re_k, calculated based on the relative velocity between the particle and the carrier phase, i.e. $\mathrm{Re}_k = \rho_\mathrm{g} d_k|\mathbf{u}-\mathbf{v}_k|/\mu_\mathrm{g}$, where μ_g is the dynamic viscosity of the gas phase. Here, the Schiller–Naumann correlation for drag is used [22],

$$C_{D,k} = \begin{cases} 0.424, & \text{for } \mathrm{Re}_k > 10^3 \\ \dfrac{24}{Re_k}\left(1+\dfrac{Re_k^{2/3}}{6}\right), & \text{for } \mathrm{Re}_k < 10^3. \end{cases} \tag{2.3}$$

Further, mass and temperature equations for an evaporating droplet are given according to the model proposed by Abramzon & Sirignano [23], assuming an infinite conductivity for the droplet. The evaporation model accounts for the effect of Stefan flow on heat and mass transfer between the droplet and the surrounding gas, assuming a dilute spray (i.e. volume fraction of the droplets below 0.1%—this allows us to use for each particle the models developed for isolated droplets) in an infinitely large domain. The rate of change of the droplet mass, m_k, is given as,

$$\frac{\mathrm{d}m_k}{\mathrm{d}t} = -\pi d_k \mathrm{Sh}^* \bar{D}_\mathrm{g} \bar{\rho}_\mathrm{g} \ln(1+B_\mathrm{M}) \tag{2.4}$$

and

$$\frac{\mathrm{d}m_k}{\mathrm{d}t} = -\pi d_k \mathrm{Nu}^* \frac{\bar{k}_\mathrm{g}}{\bar{C}_{p,F}} \ln(1+B_\mathrm{T}) \tag{2.5}$$

where $\bar{D}_\mathrm{g}$, $\bar{\rho}_\mathrm{g}$, $\bar{k}_\mathrm{g}$ and $\bar{C}_{p,F}$ are the average diffusion coefficient of the vapour in the gas mixture, density, thermal conductivity, and specific heat in the film. The parameters B_M and B_T are the Spalding mass and heat transfer numbers, and the modified Nusselt and Sherwood numbers are given as,

$$\mathrm{Sh}^* = 2 + \frac{(\mathrm{Sh}_0 - 2)}{F_M} \tag{2.6}$$

and

$$\mathrm{Nu}^* = 2 + \frac{(\mathrm{Nu}_0 - 2)}{F_T} \tag{2.7}$$

where the reference Nusselt and Sherwood numbers, Nu_0 and Sh_0, evaluated here from Frossling's correlations [24], are corrected by means of the correction factors F_T and F_M to take into account the Stefan flow, as proposed in [23]. Due to an inter dependency of B_T and B_M, an iterative solution strategy for the vaporization rate from equations (2.4) and (2.5) is used as proposed by Abramzon & Sirignano [23]. Further, given the low Biot number of the droplets in all conditions, $\mathrm{Bi}_k = hd_k/(2k_\mathrm{g}) < 0.1$, where the convective heat transfer coefficient h is computed from the Nusselt number, a convection-controlled process is assumed and, in turn, a uniform internal droplet temperature T_k can also be assumed. The rate $\mathrm{d}T_k/\mathrm{d}t$ can be obtained by an

energy balance at the droplet,

$$\frac{\mathrm{d}T_k}{\mathrm{d}t} = \frac{\dot{m}_k}{m_k c_{p,l}} \left(h_{l_v} - \frac{\bar{C}_{p,F}(T_g - T_k)}{B_T} \right). \tag{2.8}$$

In the present calculations, it is assumed that the air is initially at a homogeneous temperature T_a and pressure p_a, and contains moisture characterized by the volume fraction of water vapour $x_{\mathrm{g},w}$, which is related to the relative humidity by $x_{\mathrm{g},w} = \mathrm{RH}\, p_{w,\mathrm{sat}}/p_a$. Such conditions constitute the far-field (i.e. a region sufficiently far from the droplet surface, where the evaporation process has negligible effect) boundary conditions for droplet computations. The initial conditions of the spray are described next, in §2c.

In an initial approach, the liquid composition is considered to be pure water. To mimic the formation of a 'droplet nucleus' (i.e. what remains after evaporation has ended), the effect of non-volatile content diluted in the droplet is implemented by simply limiting evaporation of each droplet down to 6% of its initial mass, that is, $m_k/m_{k,0} = 0.06$. This value is representative of the equilibrium diameter for the range of relative humidity between 20% and 80% verified by Vejerano & Marr [13] for a model sputum droplet containing 9 mg ml^{-1} of NaCl, 0.5 mg ml^{-1} surfactants, and high protein concentration of 76 mg ml^{-1}. Nevertheless, it is worth noting that the equilibrium diameter as evaluated in the model is approximately 50% smaller for a model sputum droplet with low protein concentration (3 mg ml^{-1}) within the same relative humidity range [13]. In §2b, we provide the additional models to evaluate the effect of the droplet composition on evaporation. It should be noted, however, that neither approach considers the effect of hygroscopic growth of the droplet nuclei that may happen at high relative humidity for a recently emitted droplet, or could also be observed in a droplet nucleus undergoing changes in the relative humidity in the environment.

(b) Other effects on evaporation

It has been mentioned that the effects of solute and of the droplet curvature can determine the equilibrium size of the aerosol [14]. To account for the increase in the water vapour pressure due to the curvature of the droplet surface, Kelvin's equation [25] is employed

$$\frac{p_{\mathrm{w}}}{p_{\mathrm{sat,w}}} = \exp\left(\frac{4 M_{\mathrm{w}} \sigma_{\mathrm{l,a}}}{R\, T_g\, \rho_{\mathrm{w}}\, d_k} \right), \tag{2.9}$$

where M is the molecular weight, σ is the surface tension, R is the universal gas constant, and the subindex w represents water. The effect of the surface curvature may be enhanced due to a surface tension increase in the presence of NaCl and other components in the liquid [26], and at the same time be suppressed by the presence of surfactants which lowers the surface tension [27]. Thus, the surface tension of pure water was used as an approximation.

The saturation pressure of the water at the droplet interface is decreased by the presence of soluble as well as by insoluble substances in the droplet. To account for this in a multicomponent sputum droplet, equation (2.9) becomes [25,28,29],

$$\frac{p_{\mathrm{w}}\,(t)}{p_{\mathrm{sat,w}}} = \exp\left(\frac{4 M_{\mathrm{w}} \sigma_{\mathrm{l,a}}}{R\, T_g\, \rho_{\mathrm{w}}\, d_k} - \frac{M_{\mathrm{w}} \rho_{\mathrm{n}} d_{\mathrm{n}}^3}{\rho_{\mathrm{w}} \left(d_k^3 - d_{\mathrm{n}}^3 \right)} \sum_z \frac{\nu_{\mathrm{z}}\, \Phi_{\mathrm{z}} y_{\mathrm{z}}}{M_{\mathrm{z}}} \right) \tag{2.10}$$

where ν_{z} is the number of ions into which a solute molecule z dissociates, Φ_{z} is its practical osmotic coefficient, y_{z} is the mass fraction in terms of the total dry mass, and d_{n} is the equivalent diameter of the non-volatile nucleus n. We consider the presence of NaCl, proteins, and surfactants in the liquid. Details for the calculation of the ion-interaction parametrization of Φ_{z} for NaCl and osmotic pressure parametrization of Φ_{z} for BSA proteins are given in [28]. The latter was also used for the evaluation of that parameter in dipalmitoylphosphatidylcholine (DPPC) surfactant, considered here.

Table 1. Non-volatile composition of pure-water, high-protein sputum, low-protein sputum droplets, and molecular weight and density of each component.

	c (mg ml^{-1})			M_w	ρ
	pure water	h-p sputum	l-p sputum	(g mol^{-1})	(kg m^{-3})
NaCl salt	0	9	9	58.4	2160
BSA protein	0	76	3	66 500	1362
DPPC surfactant	0	0.5	0.5	734	1000

Finally, assuming the water as the only volatile component in the liquid droplet, it is possible to demonstrate that the rate of change of the mass fraction of water in the droplet due to evaporation is,

$$\frac{\mathrm{d}y_{\mathrm{w,k}}}{\mathrm{d}t} = \frac{m_{\mathrm{n},k,0}}{m_k^2}\frac{\mathrm{d}m_k}{\mathrm{d}t}, \tag{2.11}$$

where $m_{\mathrm{n},k,0}$ is the initial mass of non-volatile (dry) components in the droplet k.

Three different initial liquid compositions were considered, reflecting directly on the evaluation of the water vapour pressure at the droplet surface (equation (2.10)): pure water, a high protein sputum and low protein sputum. The initial concentrations and molecular weight of each component are given in table 1. The sputum compositions used in this study are those considered in [14], which are low protein content found in the nasal surface airway fluid [30], and high protein content found in breath aerosols [31], both considering a small concentration of DPPC as surfactant [32]. A homogeneous composition across all droplet sizes is considered for each case, although in reality different droplet compositions may be found depending on the origin of the droplets.

(c) Droplet size distribution and viral activity

Size distribution of droplets escaping the mouth, associated with coughing and normal paced speaking, are given as probability density functions (pdfs) of droplet diameter. These functions were obtained using the tri-modal lognormal distribution provided by Johnson *et al*. [12]. The model was named by the authors as the bronchiolar-laryngeal-oral tri-modal model, as it considers droplet production associated with three distinct modes: one occurring in the lower respiratory tract, another in the larynx, and a third in the upper respiratory tract and oral cavity, respectively. Here, we consider an initial droplet distribution in the range 1 µm–1 mm. The number concentration of droplets of size k produced in each of these modes is given as a sum over each mode i [12]:

$$\frac{\mathrm{dCn}_k}{\mathrm{d}\log_{10} d_k} = \ln(10)\sum_{i=1}^{3}\left[\left(\frac{\mathrm{Cn}_i}{\sqrt{2\pi}\ln(\mathrm{GSD}i)}\right)\exp\left(\frac{(\ln d - \ln \mathrm{CMD}_i)^2}{2(\ln \mathrm{GSD}_i)^2}\right)\right], \tag{2.12}$$

where the droplet number concentration Cn_i, the droplet mass concentration Cm_i, the geometric standard deviation GSD_i, and the count median diameter CMD_i for ith mode are given in table 2. The total number and liquid concentrations per unit volume of exhaled gas can be directly obtained by the sum of the droplet number and mass concentrations Cn_i and Cm_i, respectively, for the three modes, obtained from table 2. The mass concentrations were evaluated by [12] assuming perfectly spherical droplets and the density of pure water.

We model the virus decay in a droplet assuming an exponential decay at a rate λ such that [33],

$$\frac{\mathrm{d}N_{\mathrm{k,v}}}{\mathrm{d}t} = -\lambda N_{\mathrm{k,v}}, \tag{2.13}$$

Table 2. BLO model parameters from [12].

i	1 (B mode)	2 (L mode)	3 (O mode)
speaking			
Cn_i (# cm^{-3})	0.069	0.085	0.001
CMD_i (μm)	1.6	2.5	145
GSD_i (–)	1.3	1.66	1.795
Cm_i ($\mu g\ cm^{-3}$)	0.21	2.2	7500
coughing			
Cn_i (# cm^{-3})	0.087	0.12	0.016
CMD_i (μm)	1.6	1.7	123
GSD_i (–)	1.25	1.68	1.837
Cm_i ($\mu g\ cm^{-3}$)	0.22	1.09	69 000

where $N_{k,v}$ is the total number of *viable* viral copies (i.e. plaque forming units, or PFU) in a single droplet k. As an approximation, an exponential decay constant of $\lambda = 0.636\,h^{-1}$ is used for all droplet sizes and compositions. This value was obtained from the experiments performed by van Doremalen *et al*. [33], which verified the stability of the SARS-CoV-2 virus as an aerosol, formed of 5 μm droplets released in 65% relative-humidity ambient air. In that work, a virus half life of 1.09 h was observed. One should note that with this approach, local droplet effects such as change in solute concentrations with evaporation on virus activity are neglected. Further, the initial viral copies in each droplet is defined as

$$N_{v,k} = n_{v,0}\, V_k, \tag{2.14}$$

where V_k is the volume of the droplet. The viral load $n_{v,0}$ has been recently reported for SARS-CoV-2, with typical values found in sputum and throat swabs ranging between 10^9 and 10^4 copies ml_l^{-1} as the disease develops in sick individuals [4,6,34], who were tested daily from the on-set of the symptoms of the disease and up to several days later. Still, values as high as 10^{10} copies ml_l^{-1} were observed [34], and even 10^{11} copies ml_l^{-1} in patients who recently died [6]. Additionally, evidence of transmission caused by an asymptomatic individual has also been suggested; following the outbreak, a viral load of 10^8 copies ml_l^{-1} was detected in the individual's sputum [5]. Although the initial *viable* viral load might be lower than the values reported, these are used as a worst-case condition in the present study.

The total suspended viable viral copies and viable viral load in copies, or plaque forming units, per unit volume of liquid are

$$N_{v,s} = \sum_k N_{k,v,s} \tag{2.15}$$

and

$$n_{v,s} = \frac{\sum_k N_{k,v}}{\sum_k V_k}. \tag{2.16}$$

The infection dose of virus in viable copies needed per individual N_v^{ID} leading to the disease must be defined as a reference in order to put the results of §3a,b in context of physical distancing rules. This value is normally reported as the amount of plaque forming units which will result in a given percent responses (illness) over X% of a population—e.g. N_v^{ID50} for infection of 50% of a population. In the lack of these values for SARS-CoV-2, we used the infection dose model by

Watanabe *et al.* [35] where risk of infection P for a viral dose equal to N_v is given as

$$P = 1 - \exp\left(-\frac{N_v}{k_p}\right), \tag{2.17}$$

where k_p of 4.2×10^{-2} was obtained from the model developed for SARS-CoV-1. This was used due to the claimed similarity of this virus with SARS-CoV-2 and as it is in the same genetic group as other coronaviruses such as HCoV-229E (human common cold), MHV-S and HEV-67N (animal coronaviruses) for which the model also demonstrated a good agreement with experimental data [35]. The intervals of $N_v^{ID10} = 20$–83 PFU and $N_v^{ID50} = 130$–530 PFU are reported for a 95% confidence interval.

3. Results

(a) Ensemble averages and time scales of suspended droplet clouds

The settling of human exhaled droplet clouds is analysed in the absence of turbulence and of mean air flow, so that the effects of gravity and evaporation on various ensemble quantities of interest can be independently investigated. The Lagrangian framework, given in §2a, is considered in one (vertical) dimension and droplet clouds for two exhalation modes, speaking and coughing, are released at the height of the emitter's mouth (1.5 m) and then let settle by gravity while evaporating in ambient air. In this section, the effect of composition was not taken into account, hence droplets were considered as pure water with evaporation limited down to the equilibrium size corresponding to 6% of its initial mass.

So as to provide an overview of the evaporation-settling process, the probability density functions (pdfs) of droplet size for coughing and speaking are provided in terms of the time after emission for an ambient condition of $T_a = 20^\circ$C and RH = 60% (figure 2). These ambient conditions were chosen as a representative value of indoor spaces, especially during the winter period when the relevance of the present study is greater. In this analysis, all droplets or droplet nuclei that remain suspended in air in a given time are considered. This ensemble average is denoted by the subscript s in the quantities of interest (e.g. Ψ_s). The tri-modal bronchiolar-laryngeal-oral characteristic pdfs of droplets produced during speech and cough [12] are given at $t = 0$ s. Within one minute, most of the large droplet portion of the distribution (100 µm–1 mm) progressively disappears as these droplets reach the ground. One hour after emission, only droplets smaller than 5 µm remain suspended, that is, those typically defined as aerosol. Interestingly, at this point, the total number of particles in the sub-micrometre range is an order of magnitude higher for coughing than speaking.

Next, we evaluate the pdfs of droplet size for a suspended *and evaporating* droplet cloud—that is, considering only droplets that have not yet reached their equilibrium size or, in other words, ignoring any droplet nuclei. This condition is defined by the superscript *, as Ψ_s^*. Figure 3 shows the evolution of speech-emitted droplet pdfs evaluated for (a) the total suspended droplet cloud and (b) those evaluated for the suspended cloud minus the droplet nuclei. These are reported for the same ambient condition of figure 2. A fast change to the coughing and speaking droplet clouds occurs within the first second from emission, as droplets of the order of 1 µm fully evaporate. These small droplets quickly reach their minimum (equilibrium) size, hence determining early-on in the process the aerosol dispersion that might remain suspended in the air for much longer times. The effect of evaporation on droplet size and the resulting time scales for full evaporation for each droplet class can be more easily seen in 3*b*, as the lower limit of the given pdfs moves towards higher values as evaporating droplets reach equilibrium. The droplets within the bronchiolar mode of the probability density curve, centred at approximately 1–2 µm, have a 10 ms evaporation time scale, while those in the laryngeal mode a characterized by a longer, 1 s time scale. Moreover, figure 3*b* illustrates that the long-time scale problem may be reduced to 10 s time scale and droplets produced in the oral-mode in a virus transmission problem through droplets produced by normal, paced speech and where the presence of water is

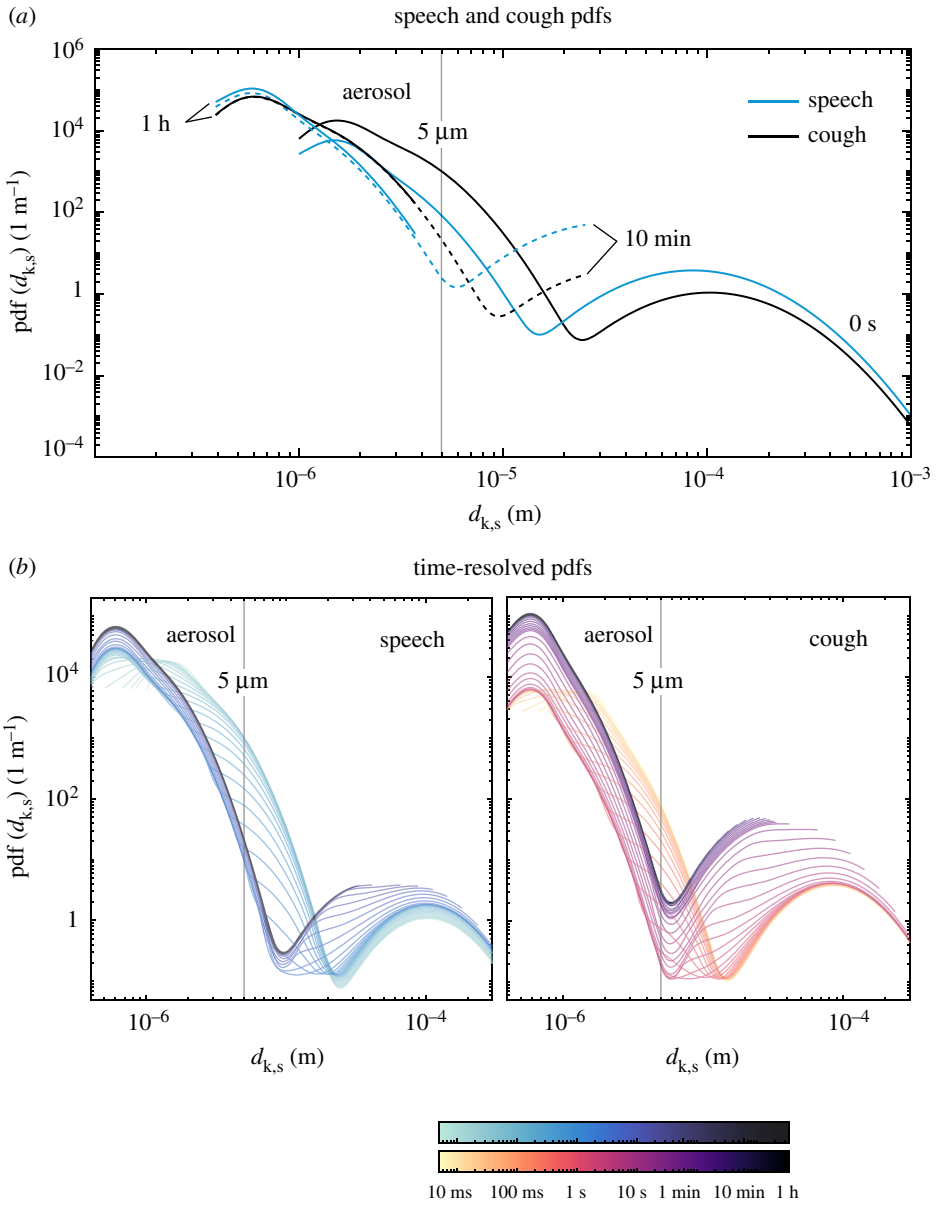

Figure 2. Evolution of the probability density function of droplet size from speaking and coughing, where (*a*) shows 0 s, 10 min and 1 h speech and cough pdfs, and (*b*) shows detailed time-resolved pdfs between 0–1 h coloured in a log scale—$T = 20^{\circ}$C, RH = 60%. (Online version in colour.)

vital to the viability of the virus in the droplet. This could be, for example, due to an increasing concentration of surfactants, salts, and other non-volatile components that can enhance viral decay [13]. In that case, droplet sizes range between 10 and 100 µm, as no droplets within the aerosol class are observed after 100 ms and any droplets larger than 100 µm are quickly deposited by gravity.

Figures 4 and 5 provide insight on the time scales needed for viral removal from the ambient air due to settling of the droplets through gravity. First, the effect of relative humidity is shown on the evolution of two ensemble quantities of the droplet clouds exhaled by speaking and coughing: mass and number of suspended droplets, both quantities normalized by their respective values

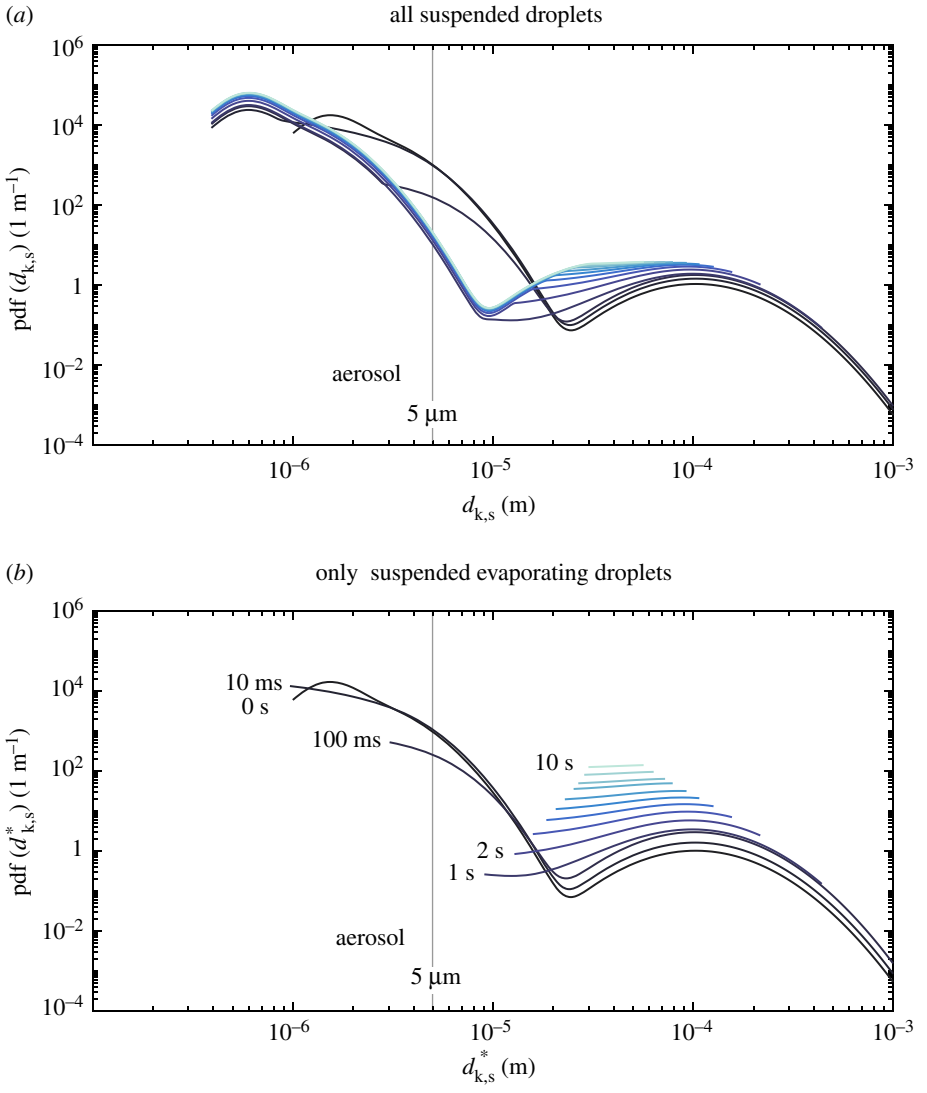

Figure 3. Evolution of the probability density function of droplet size from speaking for various times after droplets are exhaled. In (*a*) all suspended droplets are considered, and (*b*) only suspended evaporating droplets are considered (i.e. 'fully evaporated droplets that have reached their equilibrium size are removed from the pdf')—$T = 20^{\circ}$C, RH = 60%. (Online version in colour.)

at $t = 0$ (figure 4). For reference, the total mass of liquid emitted in a single cough, lasting approximately 0.5 s, is equal to that of a 30 s speech; as evaluated from the concentration distributions provided in [12] and the exhalation gas flow rates for speaking (0.211 l s^{-1}) [36] and coughing (1.251 s^{-1}) in [37]. For both exhalation modes, a significant portion of the emitted droplet cloud mass lies in the large droplets. In fact, 99% of the initial mass is concentrated in the droplet diameter range between 100 µm and 1 mm. Thus, it is not surprising that the decay of the total mass suspended relative to the initial emitted liquid mass ($m_{s,a}/m_0$, figure 4) behaves similarly in both exhalation modes. Nevertheless, what is interesting to observe in terms of the effect of evaporation and relative humidity on $m_{s,a}/m_0$ concerns the ensemble quantities for the resulting aerosol. As discussed previously, evaporation affects the small droplets in the aerosol within the first second after emission. Thus, the effect of lower (far-field) relative humidity which enhances evaporation is only noticed in the aerosol droplets within that time frame. While a

decrease of the relative mass occurs due to the evaporation of the droplets in the aerosol class, a combined increase in the aerosol mass and droplet number also occurs as larger droplets evaporate and shrink below the 5 µm diameter cut-off for aerosol.

Still in figure 4, the number droplets within the aerosol class relative to the initial number of droplets rises from 95 to 99% due to this effect, while for coughing only a small increase is observed (from 91 to 92%, roughly). As it can be inferred from figure 2, the definition of the cut-off diameter (given here as 5 µm [15] simply as a reference value) determines the total emitted amount of liquid suspended considered as aerosol—and of suspended viral copies—used in calculations of risk-based ventilation design, thus being a great source of uncertainty in such problems. The increase in $N_{s,a}/N_0$ due to evaporation in speech-emitted droplets is typically neglected but can be relevant when one assumes aerosol transmission only, say, in a well-mixed room type of ventilation problem (similar to [2]) where the intention is to evaluate risk of infection. This is aggravated by the fact that, relative to the initial emitted cloud, the number of droplets and the respective suspended mass after 1 h is an order of magnitude higher for speaking than for coughing. This analysis illustrates the risk associated with constant speaking in closed environments (as for example, in a lecture hall) due to a higher mass fraction of liquid resulting in small droplets during speaking.

(b) Considerations on the effect of droplet composition

In an attempt to provide an assessment of the uncertainty associated with the results given in §3a, we assess the effect of different droplet compositions on evaporation and, in turn, on the resulting equilibrium size of the droplets. This is discussed in terms of the ensemble quantities and time scales discussed previously. First, this issue is analysed in the context of a single droplet. Figure 6 illustrates the problem through (a) evaporation and (b) settling of a 10 µm diameter droplet. The colour lines represent different relative humidities (RH = 0–100%), while the short dash, long dash and continuum lines represent each of the compositions used: that of pure water, high-protein and low-protein sputum, respectively. For the sake of comparing the sputum droplets with pure-water droplets in figure 6, no hard limit is imposed on the minimum droplet size of pure water in this case. Hence, water droplets undergo full evaporation in less than a second, except in the case of 100% relative humidity. As the droplet evaporates, the concentration of non-volatile components increases in the droplet, thus reducing the vapour pressure at the droplet interface. Thus, a larger equilibrium diameter is reached for the case of high-protein sputum composition. As expected, evaporation is limited by the vapour pressure in the ambient. Thus, the closer to saturated air (RH = 100%), the higher is the equilibrium diameter of the droplet. Although a large variation of the equilibrium diameter was expected, observed here between 20% and 50% of the initial diameter, its impact on the settling time is quite significant. This can be seen for the 10 µm droplet by taking the respective time at the crossing of each line with the *x*-axis in figure 6*b*.

As discussed in the context of a single 10-µm droplet in figure 6*a*, the combined effect of composition and relative humidity can have a major impact on the settling time of a droplet. Next, in figure 7, we discuss this issue for the entire range of droplet sizes typically found in respiratory releases. The absolute settling times and evaporation times to equilibrium size are shown in the form of a typical Wells curve in (a), both in terms of the droplet size, for high- and low-protein sputum droplets, and different relative humidities. The relative difference between the settling time between each composition is given on the right-hand axis of (b). Settling times of droplets in the 1–50 µm range are strongly affected by composition, while this effect is negligible in droplets larger than 100 µm. Considering a droplet of 20 µm, the approximate average-sized droplet in [13], the time for full evaporation until equilibrium was found in the present study to be between 0.8 and 2.8 s for relative humidities between 40 and 80%, respectively. These time scales correspond to roughly 10 times higher evaporation rates in the present work than those found under quiescent conditions of a droplet cluster over a hydrophobic surface using a fluid with same composition of the present study. Further, in the transition range between 50 and 100 µm,

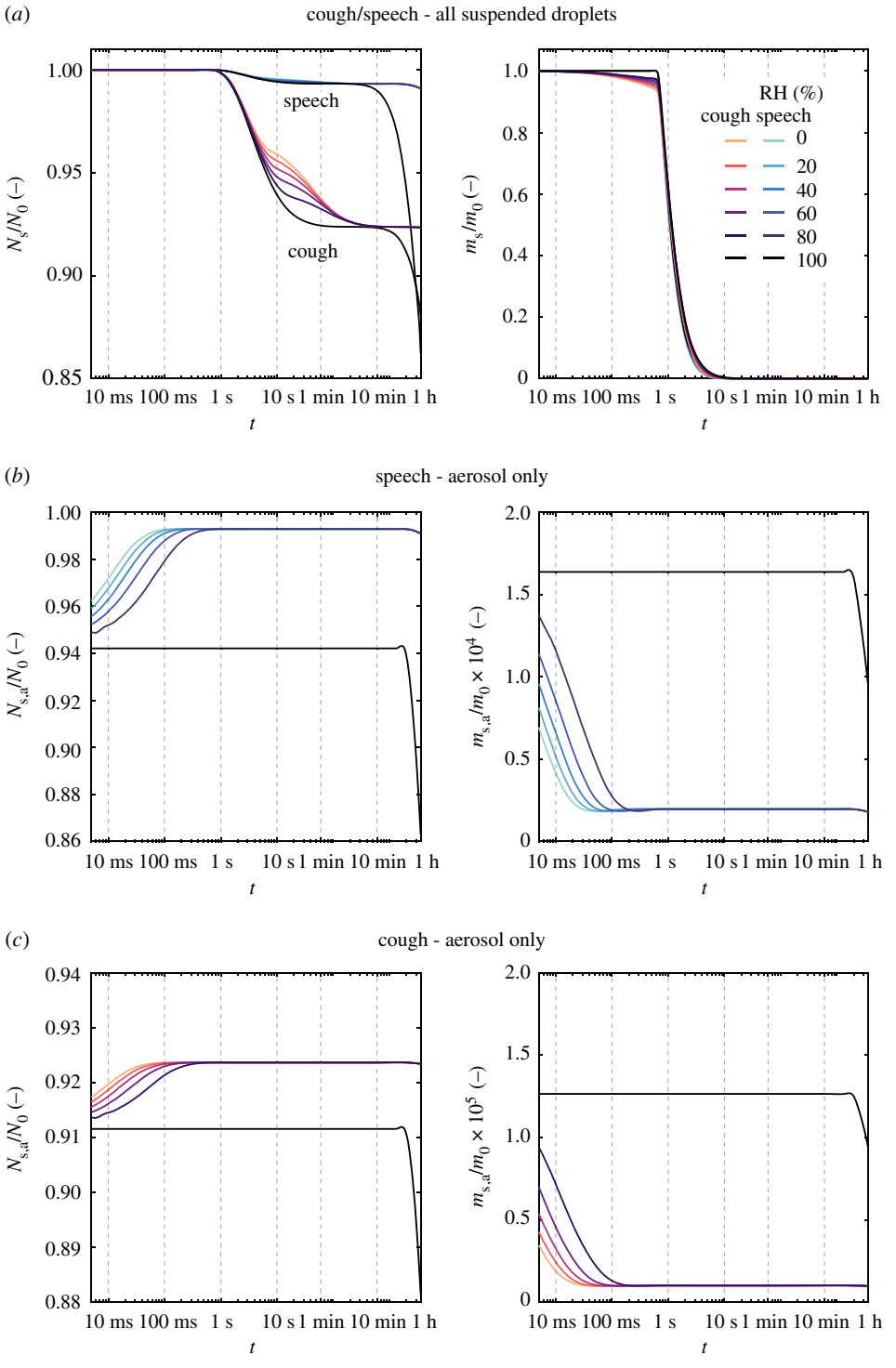

Figure 4. Time evolution of ensemble quantities (total mass and number) normalized by the respective value at $t = 0$ for sprays exhaled by speech and cough—$T = 20^{\circ}$C, RH = 0–100%. In the top row, ensemble quantities shown are evaluated for all suspended droplets, while in the middle and lower low the quantities are calculated considering only droplets below 5 µm. More detail on the time evolution of m_s/m_0 is provided in figure 5. (Online version in colour.)

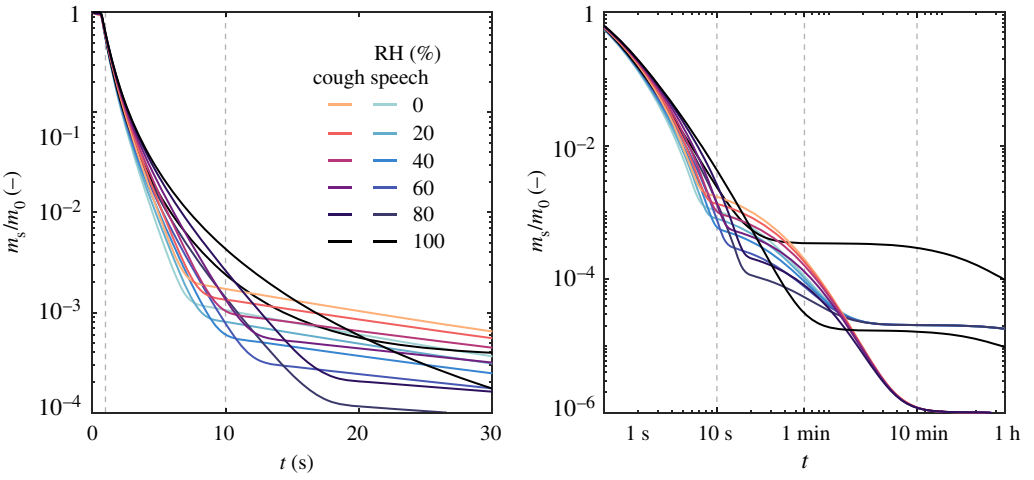

Figure 5. Detail of the time evolution of total mass normalized by the respective value at $t = 0$ shown in figure 4. The left-hand side plot is given in a linear time scale up to 30 s, while the right-hand plot is given for a log scale up to 1 h. (Online version in colour.)

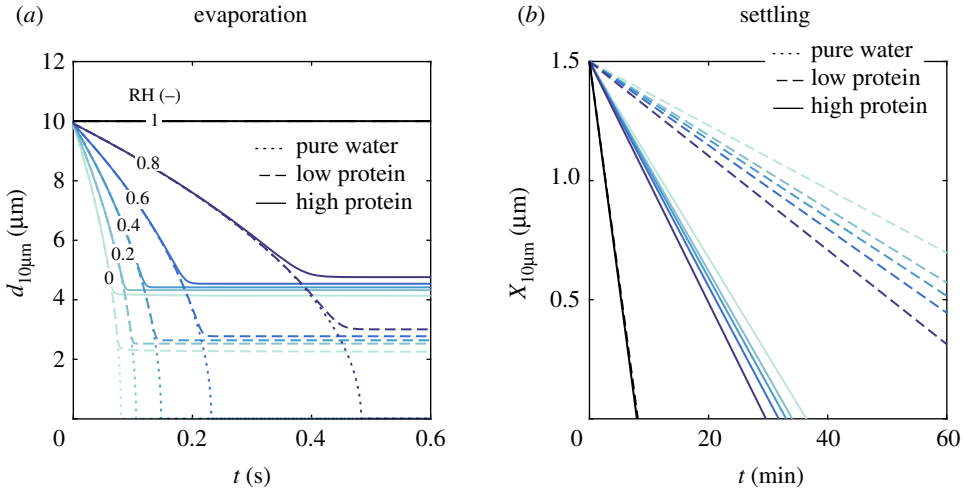

Figure 6. Impact of the droplet composition modelling approach (pure water; sputum 9 mg ml^{-1} NaCl, 3 mg ml^{-1} protein; sputum 9 mg ml^{-1} NaCl, 76 mg ml^{-1} protein) on the (*a*) evaporation and (*b*) settling of 10 µm droplets under different relative humidities. The relative humidity is shown in colour (RH = 0–100%)—$T = 20^{\circ}$C. (Online version in colour.)

the deposition and evaporation time scales found in this work were similar, hence the effect of composition swiftly disappears once the settling time due to gravity becomes much shorter than the droplet evaporation time scale.

There are key implications of the above findings. Although, at a first glance, one would be tempted to neglect the composition effect in the gravity-controlled short-time scale viral transmission problem (i.e. the ballistic and exhaled gas-driven motion of large droplets), significant differences in settling time and size in the 50–100 µm range can be critical. Such droplets might remain longer in air at face height, being more likely to be inhaled by someone near a sick individual. This problem has a direct impact on the uncertainty of methods to evaluate the safe physical distancing and, therefore, should be further investigated for better understanding, for example by means of high-fidelity flow simulations. Besides the short-time scale implications, the large differences in deposition times of droplets in the aerosol class, as an effect of both

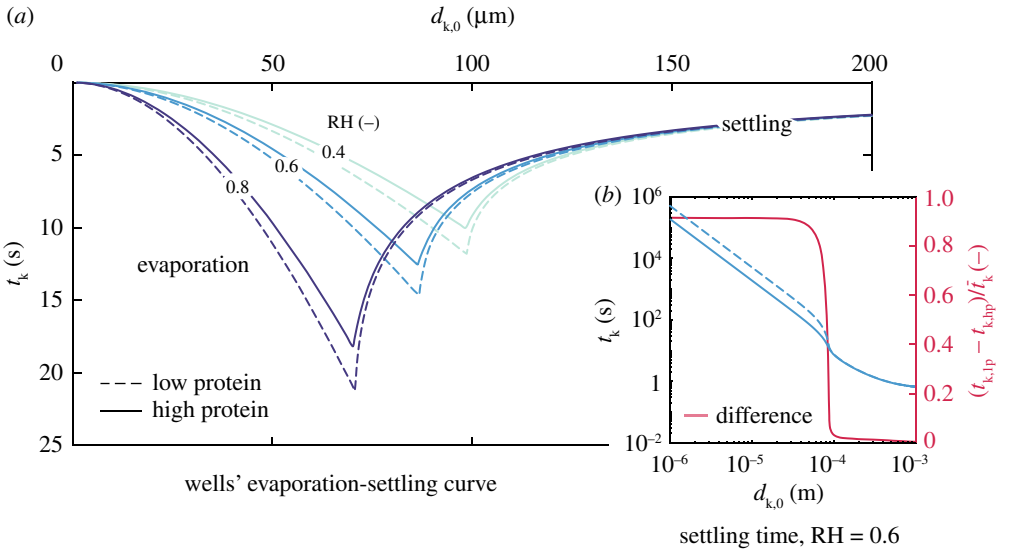

Figure 7. The (*a*) Wells' evaporation-settling curve showing the time for either full droplet evaporation to its equilibrium size or its settling time to the ground for $T = 20^{\circ}$C, RH = 40, 60 and 80%, and two saliva compositions: low protein sputum (9 mg ml^{-1} NaCl, 3 mg ml^{-1} protein) and high protein sputum (9 mg ml^{-1} NaCl, 76 mg ml^{-1} protein). In (*b*), the settling times for each composition (left axis) and their respective relative differences (right axis) are given for RH = 60%. Significant effect of composition on settling time scales depends on relative humidity, and is observed in droplets up to 100 μm, approximately. (Online version in colour.)

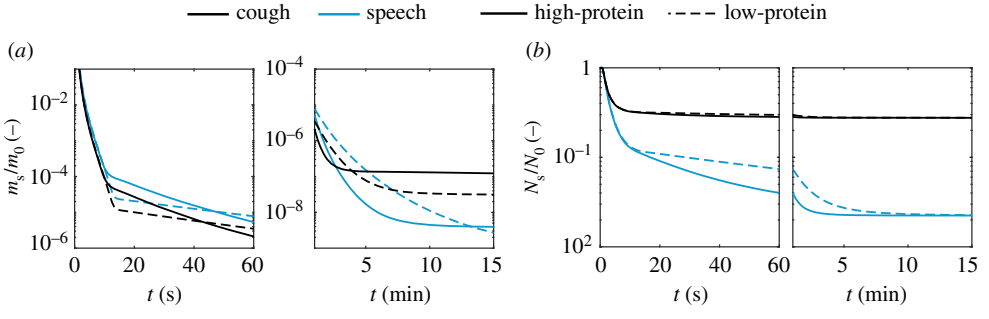

Figure 8. Time evolution of (*a*) total mass and (*b*) total droplet number, all normalized by their respective values at $t = 0$, in terms of the composition: low protein (sputum 9 mg ml^{-1} NaCl, 3 mg ml^{-1} protein) and high protein (sputum 9 mg ml^{-1} NaCl, 76 mg ml^{-1} protein)–$T = 20^{\circ}$C, RH = 60%. (Online version in colour.)

relative humidity (figure 6*a*) as well as composition (figure 7*b*), might also affect the long-time scale problem, that is, the virus removal by ventilation in indoor spaces. This large difference can be clearly seen at large times in terms of m_s/m_0 and N_s/N_0 (figure 8) not only due to the significantly longer deposition times of such droplets, but also due to the difference in the mass that can remain suspended. Some of these issues are explored next, in §3c

(c) Suspended viable virus

In this section, the evolution of the total number of suspended viable viral copies is evaluated for speaking and coughing. We consider a single cough in which all droplets are assumed to be released instantly, and continuous speaking in which the droplets are considered as uniformly

emitted over its duration. Assuming a short 0.5 s cough with a mean volumetric gas flow rate of 1.25 l s^{-1} [37], the total emitted liquid can be directly obtained from the total exhaled volume of gas and the liquid concentration values available in table 2. Similarly, we consider the case of continuous, paced speech over 30 s at an average volumetric gas flow rate of 0.211 l s^{-1} [36]. Hence, both exhalation modes result in the *same* emitted liquid mass. Additionally, for this analysis, we consider two sputum compositions (high- and low-protein sputum) and assume a range of low and high viral loads at the emission source to be that of a symptomatic person in: (i) a few days after the symptoms appear (typically 10^8 copies ml$_l^{-1}$) and (ii) at a severe stage in the disease (10^{11} copies ml$_l^{-1}$). The evolution of the total number of suspended viable copies of virus $N_{s,v}$ is given for those conditions and 40 and 80% relative humidity (figure 9). As a reference value, the infection doses N_v^{ID10}, N_v^{ID50} and N_v^{ID100} are also given. For speaking, an additional plot is given with a time scale relative to the end of the 30 s speech (figure 9*b*).

One of the key differences in the decay of suspended virus emitted from (a) coughing in comparison to (b) speaking can be seen in respect to N_v^{ID100} in figure 9. For a cough and the worst-case viral load scenario (10^{11} copies ml$_l^{-1}$), the viral inactivation and removal through gravity will quickly bring the total $N_{s,v}$ down to values below those needed for 100% risk of infection (if the whole amount is inhaled by person) in about 1–7 min. By contrast, 30 min are needed for reduction to the same $N_{s,v}$ levels in speaking. Due to the small droplets produced in speaking, a high viral dose can still be suspended up to 1 h—although this is approximately the half-life of the virus—being one order of magnitude higher than in coughing at that time.

To discuss the evolution of the total number of suspended viable copies of virus in the context of indoors activities, we consider just droplets at face height (between 1.2 and 1.8 m) in figure 10. Based on the results of figure 9, here, we assume a worst-case scenario in terms of droplet removal by gravity, that is, a droplet composition of low-protein sputum and relative humidity of 40%. In terms of the virus load in sputum, a typical case of the disease is considered, that is, a high viral load in a patient after a few days of the first symptoms of the disease ($n_{v,0} = 10^9$ copies ml$_l^{-1}$). Three cases of upward, zero and downward flow are then evaluated by setting the mean vertical gas velocity as $+0.1$, 0, and -0.1 m s^{-1}. These simple cases aim to illustrate possible flow conditions that may arise in indoors activities (e.g. thermal plume, heating systems or flow streams caused by ventilation systems). The effect of the mean flow on viral removal at face height is evident: downward flow can reduce the suspended viral dose to safe levels in only a couple of seconds, while upward flow may actually worsen the problem by keeping a higher viral dose suspended at face height for several minutes longer than no flow at all. Moreover, figure 10 also illustrates the risk associated with speech-emitted droplets in the short-time scale problem; this will be discussed in detail in the next section, as we consider the gas exhaled during speech.

(d) Implications for physical distancing policies

In this section, where applicability of previous results concerning the suspended amount of viable virus and the respective time scales are demonstrated in the context of physical distancing and ventilation by considering three canonical fluids problems. One should note that for such demonstration, some simplifications of the physics involved in each of the problems are made; these are highlighted throughout the section.

(i) Uniform velocity

In a setting which the initial velocity of the exhaled gas carrying the droplets can be ignored—this might be a good assumption in, say, slow speaking or exhalation in the presence of a strong background airflow—the above time scales can be easily translated into information on space. For example, assuming a uniform velocity U_{AB} from emitter A to receptor B located a distance L from A in the airflow direction, the total suspended liquid mass can be found by simply setting $t = L/U_{AB}$ in figure 5. For instance, for $U_{AB} = 0.5$ m s^{-1} and $L = 2$ m, $t = 4$ s and hence about

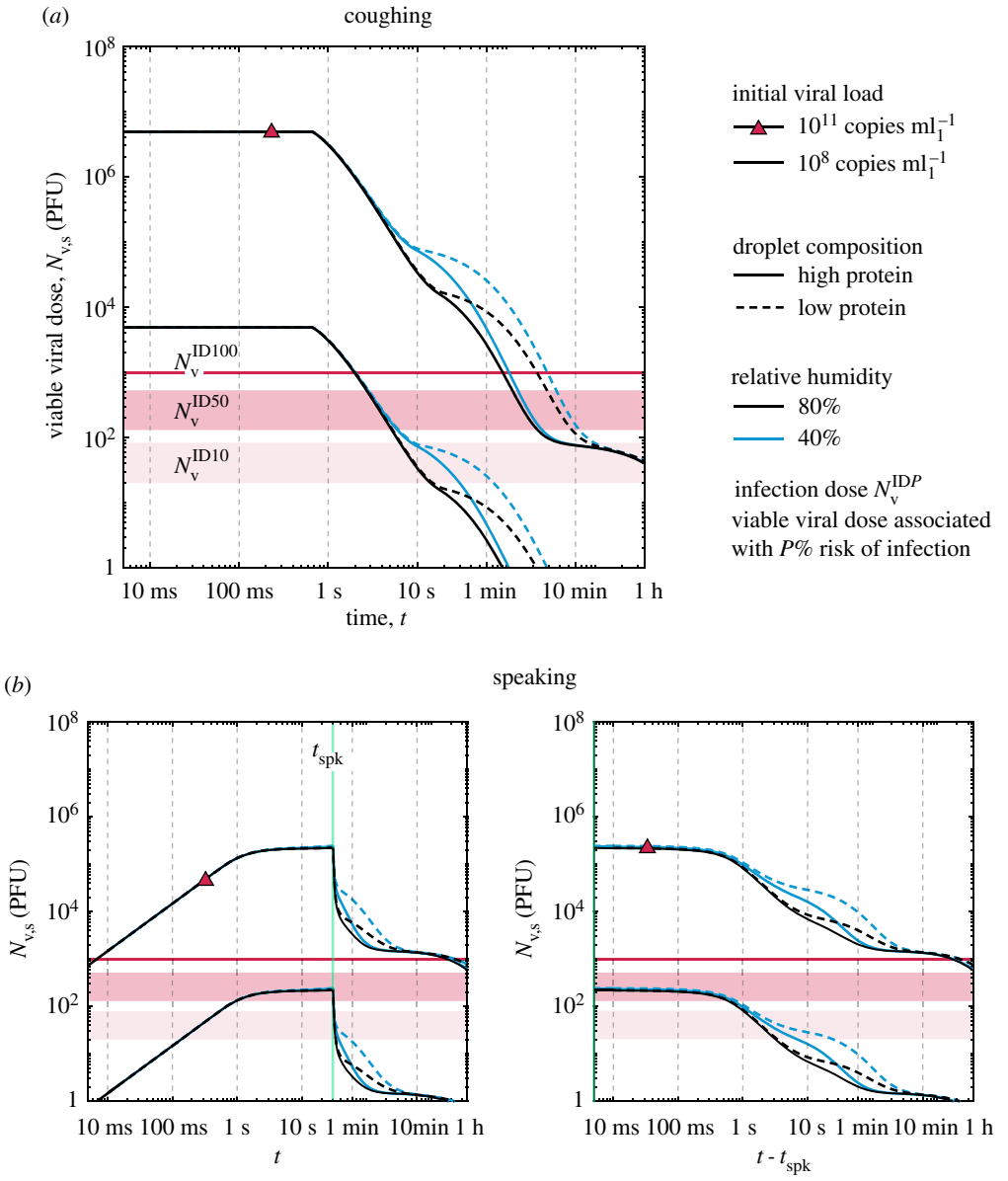

Figure 9. Evolution of the suspended viable viral dose following (*a*) a short cough and (*b*) 30 s speech in terms of two droplet compositions (low- and high-protein sputum), RH = 40 and 80%, and low (10^8 copies ml$_l^{-1}$) and high (10^{11} copies ml$_l^{-1}$) initial viral load $n_{v,0}$. (Online version in colour.)

7×10^{-3} to 2×10^{-2} of the initial liquid is still in the air, depending on the ambient conditions. Similarly, in terms of virus dose (figure 10), an amount up to 100 PFU could be available at face height, depending on specific flow conditions, which illustrates that a 2 m safe distance may not be adequate without the use of protective mask/respirator for the case of strong convection from the emitter to the receptor.

(ii) Jet decay

Speaking or coughing involve high velocities at the mouth, which then decay as the flow evolves downstream from the emission source. Here, we model a respiratory emission as a continuous round jet in stagnant ambient air. Although, in reality, the emission is not continuous and the jet

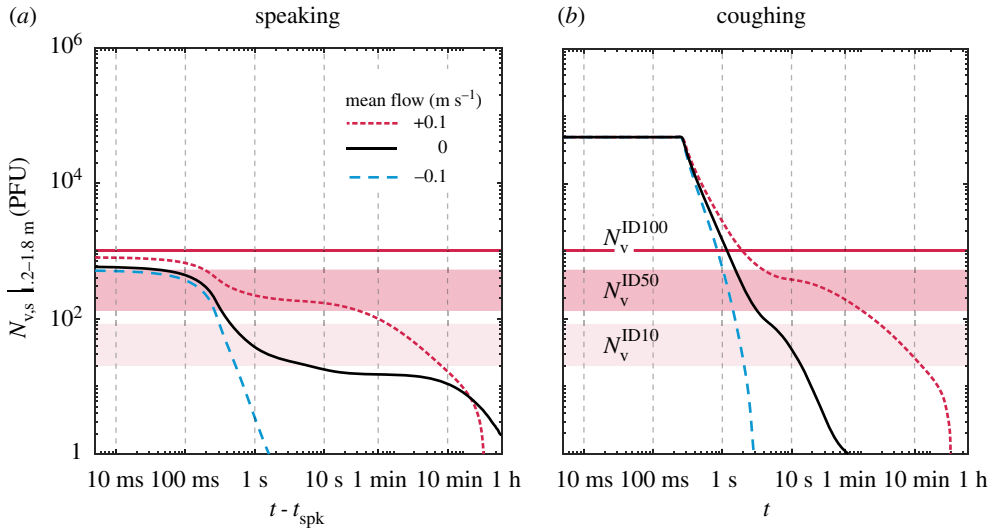

Figure 10. Evolution of the suspended viral dose at face height (between 1.2 and 1.8 m) following (*a*) 30 s continuous speech and (*b*) a short cough (i.e. same exhaled liquid mass) for three cases of ambient mean flow: upward (+0.1 m s^{-1}), zero, downward (−0.1 m s^{-1})—low-protein sputum, (RH = 40%, $n_{v,0} = 10^9$ copies ml$_l^{-1}$). (Online version in colour.)

is buoyant and behaves like a starting jet of finite duration, the duration of the release, especially for speaking or breathing out, could last of the order of seconds. Other effects such as turbulence [17] and entrainment of ambient air [18] are expected to affect droplet evaporation and settling times. Nevertheless, for the duration of the release, it may not be a bad approximation to consider the decay of a continuous round jet, which allows us to build an easy-to-use connection between the settling times of §3a with a time-of-flight estimate to reach the safe distance L_{sf}. The mean velocity U at the centreline of an axisymmetric turbulent jet decays as:

$$\frac{U}{U_0} = C\left(\frac{x}{D}\right)^{-1} \tag{3.1}$$

where L is the distance from the jet's source, D the jet diameter, U_0 the velocity at the release, and $C \approx 6$ is an empirical constant from experiment [38] (the non-circular mouth opening can be absorbed as a first approximation into the value of the constant C). Following a fluid particle travelling along the central streamline of the jet,

$$\frac{\mathrm{d}L}{\mathrm{d}t} = U \Leftrightarrow L^2 = 2\,C\,D\,U_0\,t_{fl}, \tag{3.2}$$

which relates the mean time of flight t_{fl} needed to reach a distance L. For $L = L_{sf} = 2$ m, $U_0 = 5$ m s^{-1}, $D = 10$ mm, values typical of speaking [36], the physical distancing limit $L_{sf} = 2$ m is reached at $t_{fl} = 6.7$ s. The results of §3a suggest that when speaking more than about 10^{-3} of the emitted release has not yet fallen on the ground at 2 m.

Assume that the steady-state velocity decay (equation (3.2)) is also valid for a cough. Using $U_0 = 20$ m s^{-1} and $D = 20$ mm, a distance of $L = 2$ m is reached at about $t_{fl} = 0.8$ s. Figure 9 shows that by that time there has been virtually no gravitational removal when considering the total suspended liquid, and figure 10 shows that between 1.2 and 1.8 m, at face height, an order of magnitude removal is observed. Hence, the receptor will receive a significant proportion of all viral load directly at face height. Safe levels are reached only after 30 s–1 min of flight time for either zero or downward flow, which suggests that an unprotected cough is not safe at any reasonable distance.

Speaking for 30 s (figure 9) with the high-concentration estimate of viral load releases enough virus particles that, even after 10 min, the suspended particles are still above the smallest dose

needed for 100% risk of infection. However, with the 10^8 copies $\mathrm{ml}_\mathrm{l}^{-1}$ estimate, the suspended viable dose has fallen by about two orders of magnitude within a few minutes. For aerosol droplets in particular, removal by gravity starts only after 20 min with the gravitational settling rate reaching a steady-state value of about $\kappa = 0.39\,\mathrm{h}^{-1}$ ($\kappa = 0.13\,\mathrm{h}^{-1}$ for suspended aerosol droplets by coughing) after 30 min. Both viral inactivation and removal by gravity have a small cleansing effect for the aerosols; hence ventilation removal must be added if continuous speaking is to be safe.

Furthermore, recent work suggests that the voice loudness can enhance droplet production during speaking [39], and that a high viral replication and the highest viral loads of SARS-CoV-2 were found to occur in the throat—where fine droplets are produced—in the early stages of the disease (or in asymptomatic individuals) [4]. Considering such findings in a worst-case scenario of virus loads and potentially greater amounts of droplets emitted in a loud environment, the potential of speaking as a mechanism of indoor as well as outdoor viral transmission becomes even more evident. This corroborates the suggestion that aerosol transmission was the main contagion mechanism in a number of cases, such as the restaurant in Guangzhou (China) and the choir rehearsal in Valley Chorale (USA) as recently suggested in [1].

(iii) Mixing ventilation

In the case of mixing ventilation—for instance, through ceiling-placed A/C systems, fan-assisted, natural or jet-induced ventilation—it may be assumed that the air in the room is homogeneously mixed very quickly, typically of the order of the turbulent turnover time $T_\mathrm{turb} = L_\mathrm{turb}/u'$, where L_turb is the integral length scale (roughly 0.5–1 m for a typical room) and u' the characteristic turbulent velocity (roughly 0.02–0.05 m s^{-1}). Hence, the mixing timescale may be of the order of 1–50 s. This is short compared to a typical purge time of the room by fresh air, which is the inverse of the 'air changes per hour' (ACH) that typically characterizes ventilation systems. Targets for well-ventilated rooms are 10–20 ACH, which suggests an average purge (or residence) time T_res of 180–360 s. Therefore, considering the typical ACH values, the well-mixed approximation is fair. The $N_\mathrm{v,s}$ removed by ventilation would be given by $\mathrm{d}N_\mathrm{v,s}/\mathrm{d}t = -N_\mathrm{v,s}(T_\mathrm{res})^{-1}$, where $T_\mathrm{res} = 1/\mathrm{ACH} = V/Q$, with V the volume of the room and Q the ventilation volume flow rate. This gives an exponential decay with T_res as the characteristic timescale. For example, a removal of 10^{-4} of the original $N_\mathrm{v,s}$, associated with the aerosol would be reached at a time $t \approx 9\,T_\mathrm{res}$.

Consider an indoor environment with a total volume $V = 200\,\mathrm{m}^3$ with a room height of 2.5 m, simulating a lecture room, and one infected individual continuously speaking for 1 h. The well-mixed approximation results in an uniform concentration of suspended viral aerosol droplets that are generated by speaking and reduced via simultaneous ventilation removal, viral inactivation and gravity. The total suspended viable viral copies is then given by

$$\frac{\mathrm{d}N_\mathrm{v,s}}{\mathrm{d}t} = \dot{N}_\mathrm{v,gen} - \left(\lambda + \kappa + (T_\mathrm{res})^{-1}\right)N_\mathrm{v,s}, \tag{3.3}$$

where $\dot{N}_\mathrm{v,gen}$ a generation rate and κ a gravitational settling rate defined in §3d(ii). We approximate $\dot{N}_\mathrm{v,gen}$ via computations similar to those used to obtain figure 9*b* while only considering aerosol particles that can follow the airflow within a room. As discussed in §3a, the choice of cut-off diameter for aerosol introduces great uncertainty and should normally be subject to ambient and local flow conditions, together with droplet composition. For the sake of this analysis, a 5 µm diameter cut-off is considered as a reference for consistency with [15]. Hence, $\dot{N}_\mathrm{v,gen}$ could be estimated at a given time after emission when viral decay had little effect and the number of suspended viable viral copies bounded to aerosol particles was approximately steady (at about $t - t_\mathrm{spk} = 2$–3 min for high protein sputum and RH = 40–80%). Assuming a range of 10^8–10^{10} copies $\mathrm{ml}_\mathrm{l}^{-1}$ virus load in the sputum of the infected individual, then $\dot{N}_\mathrm{v,gen}$ is in the range of about 0.05–4.67 PFU/s.

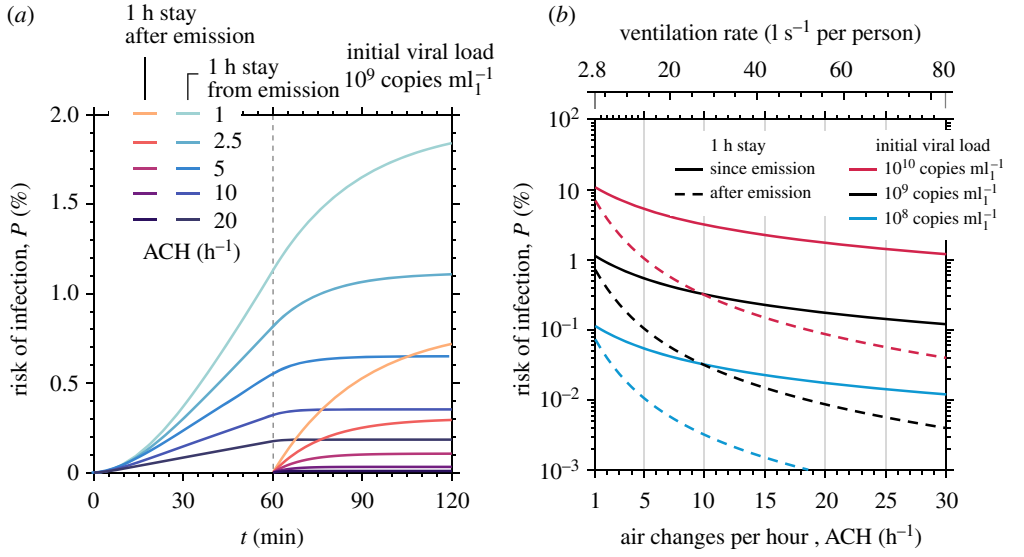

Figure 11. Infection risk in terms of (*a*) exposure time and (*b*) ventilation rate in a 200 m^3 room with one infected occupant. (Online version in colour.)

Following the calculation of equation (3.3), for an occupant inhaling 0.521 l s^{-1} [36], the infection dose model by [35] (see also equation (2.17)) yields an infection risk of about 0.1–10.7% at the end of a 1 h emission period, when the room is ventilated with 1 ACH (i.e. about 2.8 l s^{-1} per person for a typical 1 person/4 m^2 occupancy density corresponding to 20 occupants). The infection risk may increase to 0.2–17% if one occupant spends another hour in the same room. For a well-ventilated room with 10 ACH (i.e. about 28 l s^{-1} per person), the infection risk reduces to 0.03–3.2%, which confirms the importance of ventilation in mitigating risk from long-time emission, especially when the emitter is pre-symptomatic or asymptomatic, that is, typically having a lower viral load. However, to ensure a higher cleansing effect, reducing risk to levels well below 0.5% for any viral load in the considered range, one would need O(100) ACH. This value, that is an order of magnitude stronger than even those found in hospital settings, shows that ventilation only is not enough to completely suppress infection risk, highlighting the importance of face coverings and additional complementary protection measures.

The risk estimations described above are also corroborated in figure 11, where a wide range of ventilation rates is considered. As shown in figure 11*a* for a nominal viral load, the infection risk is a strong function of the exposure time and ventilation rate. Even after the end of the 1 h emission period (where $\dot{N}_{v,gen} = 0$), the existing concentration of suspended viable viral copies can significantly raise the risk of infection for an occupant present in the room since the start of the emission. This is also true for an occupant entering the room only after 1 h (as also depicted in figure 11*a*). For high ventilation rates, the purging time is small so that complete removal of aerosols is achieved quickly. However, when lower ventilation rates are employed, complete removal by the combination of ventilation, viral decay and gravitational settling shows a time delay that could be of the order of a few minutes or hours. Therefore, in practical settings with low ventilation rates, infection risk would also be a function of occupancy in the room.

One should note that the absolute risk calculated in figure 11 is specific to the model room and number of infected individuals considered here. However, the insights obtained from the suspended viable virus calculations and the consequent estimates of $\dot{N}_{v,gen}$ and κ can be applied to different scenarios using equation (3.3) or can be used in conjunction with other methods. For settings where the well-mixed approximation does not necessarily hold, e.g. when displacement or mixed-mode ventilation is employed, methods and models that can also incorporate flow

effects induced by ventilation or stratification [40] and movement of people [18] should be considered.

Based on the previous mixing ventilation estimates, typical regulations for safe ventilation practices seem satisfactory in reducing infection risk. This corroborates the guidelines put forward by [41] that typical indoor spaces regularly attended by the same group of people, e.g. office spaces or school classrooms. According to [41], these should adhere to existing ventilation guidelines ($10\,l\,s^{-1}$ per person [42] and $5–10\,l\,s^{-1}$ per person [43] for offices and school classrooms, respectively) while keeping to normal occupancy densities so that infection risk posed by the long time scale airborne particles remains low for typical usage conditions. Nevertheless, if attention is given to emitters with potentially higher viral loads, or indoor spaces with an unusually high amount of infected individuals, indoor air exchange rates should be increased by an order of magnitude, exposure time should be limited, or more effective ventilation systems should be put in place.

4. Conclusion

A comprehensive modelling strategy of the evaporation and settling of droplets emitted in respiratory releases (speaking, coughing) was provided in a Lagrangian framework, which included state-of-the-art models for droplet evaporation, effects of the sputum composition on heat and mass transfer, and droplet size distributions. By considering characteristics of the SARS-CoV-2 virus, such as its decay rate, viral load in infected individuals, and estimated infection dose from SARS-CoV-1, theoretical estimates were given for the evolution of the droplet cloud in terms of suspended mass and droplet number and its associated viable viral dose, for a short cough and in continuous, paced speech. Such metrics were then used in the context of canonical problems providing insights on physical distancing and ventilation.

The evolution of the probability density functions of droplet size given by the bronchiolar-laryngeal-oral tri-modal model for speaking and coughing were evaluated. Evaporation time scales of approximately 100 ms and 1 s were observed for droplets within the bronchiolar mode (centred at 1–2 µm) and the laryngeal mode (centred at 6–8 µm), respectively. Large droplets produced in the oral mode (centred at 100–200 µm) were observed to settle by gravity within just a few minutes. Evaporation and settling time scales of the droplets were strongly impacted by the sputum composition, which limited the resulting equilibrium size of the generated droplet nuclei (i.e. 'dry droplets'). Varying the droplet composition and the ambient relative humidity, resulted in 90% relative differences in the settling times for droplets up to approximately 100 µm, thus impacting the evolution of the droplet cloud and its associated viral dose. The observed time scales were found to be typical of droplets in respiratory releases [11]. Still, new free falling multi-component single-droplet experiments under well-controlled ambient conditions are required to assess the precision of the modelling strategy used.

About 1 h after emission, virtually all mass lied in droplets within the aerosol class between 0.4 and 4 µm in diameter. Although, in absolute terms, a short cough emitted as much liquid mass as 30 s of continued, paced speaking, the resulting aerosol contained an order of magnitude more mass for speaking than coughing. Further, the effect of an upward mean ventilation flow was observed to sustain a higher viral dose at face height, increasing to 5 min the time at which an infection dose for 10% infection risk was found suspended, in relation to 1 s and 10 s for speaking and coughing when only gravity was considered. At 10 min after emission, the largest droplets in the cloud were just above 10 µm. These results stress the need for air change through ventilation to reduce the risk of disease transmission in indoors activities, and emphasize the importance of the direction of displacement ventilation and precise account of the aerosol characteristics.

Due to the high associated mass and viral dose in large droplets (approx. 99% of the emitted value), both a short cough and continued speaking were found to be unsafe within 2 m without personal protective equipment. In this case, the problem is governed by the settling of large droplets ($d_k > 100\,\mu m$) produced in the oral mode, hence the effect of droplet evaporation and composition were negligible. Upward air streams resulting from displacement ventilation could

increase the distance travelled by droplets, while downward streams (e.g. from under-floor negative pressure ventilation systems) could be used to enhance droplet removal from face height. As ventilation is of utmost importance for aerosol removal, personal protective equipment is crucial to reduce the risk of short-range contamination in ventilation systems inducing upward flows.

The implications of the present findings for virus transmission control measures are:

— Standing 2 m opposite an infected speaker is not safe without the use of a protective mask or respirator. In the presence of a constant mean flow ($U_{AB} = 0.5\,\mathrm{m\,s^{-1}}$), it was found that up to 100 viable viral copies were within face height after just a few seconds. In the absence of such flow, jet-decay calculations demonstrated that a similar viral dose can be found at face height at the same 2 m distance, corresponding in 10% risk of infection, while for a short cough the suspended dose would lead to 50% risk.
— An unprotected cough is not safe at any reasonable distance close to an infected individual. Jet decay estimates showed that even for an initial viral load of 10^8 copies $\mathrm{ml_l^{-1}}$, equivalent of that found in infected asymptomatic individuals, safe levels of infection at 2 m from emission are only attained after 30 s to 1 min of flight time at face height.
— Settling of the aerosol by gravity was found to be small compared to the viral decay. For the suspended aerosol resulting from speaking, removal by gravity started only after 20 min and stabilized at settling rate of $\approx 0.39\,\mathrm{h^{-1}}$ after 30 min ($0.13\,\mathrm{h^{-1}}$ for coughing). Therefore, gravitational settling cannot be relied upon for reducing the infection risk posed by aerosols.
— The presence of air currents strongly affects the suspended viral dose regardless of the exhalation mode. A $0.1\,\mathrm{m\,s^{-1}}$ downward flow can remove completely suspended virus in less than 10 s, while a $0.1\,\mathrm{m\,s^{-1}}$ upward air stream can maintain at face height a viral charge corresponding to 50% infection risk for ≈ 1 min, and a viral charge corresponding to 10% infection risk for ≈ 10 min.
— An infected person speaking for 1 h in a model room may lead to infection risk levels of 10–20% with inadequate ventilation, but the risk can be reduced by, at least, a factor of three if 10 air changes per hour are employed. Ventilation (in terms of both magnitude and direction) is of utmost importance in minimizing infection risk indoors.

The present results illustrate the need of addressing the problem between the short and the long time-scale settling, that is, between what is commonly defined as droplet transmission and aerosol transmission ($d_k < 5\,\mu$m, [15]). The concerning time scales observed are 10 s–10 min, in which the droplet cloud is characterized, in addition to the aerosol class, by 5–100 μm droplets. Although these droplets represented just under 1% of the total initial mass and viral dose emitted, this value is roughly 30 times more than what lies in the aerosol class. Within this time scale, effects of composition and of relative humidity played an important role resulting in order-of-magnitude variations of the estimated suspended mass and viral dose.

Data accessibility. The code for the model described in §2 is publicly available on GitHub [44].

Authors' contributions. E.M. and P.M.O. conceived the work. All authors contributed to the calculations, analysis, and writing and revision of the manuscript. The final version of the manuscript was approved by all authors, who are accountable for all aspects of the work.

Competing interests. We declare we have no competing interests.

Acknowledgements. The authors kindly thank Dr M.P. Sitte for his assistance with the Abramzon-Sirignano model and Dr A. Boies and Dr M. Davies Wykes (University of Cambridge), Prof. C. Noakes (University of Leeds), Dr H. Burridge and Dr. M. Stettler (Imperial College) for their useful comments. The network formed under the auspices of the Rapid Assistance in Modelling the Pandemic (RAMP) initiative coordinated by the Royal Society is also acknowledged.

References

1. Dancer S, Tang J, Marr L, Miller S, Morawska L, Jimenez J. 2020 Putting a balance on the aerosolization debate around SARS-CoV-2. *J. Hosp. Infect.* **105**, 569–570. (doi:10.1016/j.jhin.2020.05.014)
2. Buonanno G, Stabile L, Morawska L. 2020 Estimation of airborne viral emission: quanta emission rate of SARS-CoV-2 for infection risk assessment. *Environ. Int.* **141**, 105794. (doi:10.1016/j.envint.2020.105794)
3. To KKW *et al.* 2020 Temporal profiles of viral load in posterior oropharyngeal saliva samples and serum antibody responses during infection by SARS-CoV-2: an observational cohort study. *Lancet Infect. Dis.* **20**, 565–574. (doi:10.1016/S1473-3099(20)30196-1)
4. Wölfel R *et al.* 2020 Virological assessment of hospitalized patients with COVID-2019. *Nature* **581**, 465–469. (doi:10.1038/s41586-020-2196-x)
5. Rothe C *et al.* 2020 Transmission of 2019-NCOV infection from an asymptomatic contact in Germany. *N. Engl. J. Med.* **382**, 970–971. (doi:10.1056/NEJMc2001468)
6. Pan Y, Zhang D, Yang P, Poon LL, Wang Q. 2020 Viral load of SARS-CoV-2 in clinical samples. *Lancet Infect. Dis.* **20**, 411–412. (doi:10.1016/S1473-3099(20)30113-4)
7. Zou L *et al.* 2020 SARS-CoV-2 viral load in upper respiratory specimens of infected patients. *N. Engl. J. Med.* **382**, 1177–1179. (doi:10.1056/NEJMc2001737)
8. Wells WF. 1934 On air-borne infection: study II. Droplets and droplet nuclei. *Am. J. Epidemiol.* **20**, 611–618. (doi:10.1093/oxfordjournals.aje.a118097)
9. Xie X, Li Y, Chwang ATY, Ho PL, Seto WH. 2007 How far droplets can move in indoor environments. *Indoor Air* **17**, 211–2256. (doi:10.1111/j.1600-0668.2007.00469.x)
10. Papineni RS, Rosenthal FS. 1997 The size distribution of droplets in the exhaled breath of healthy human subjects. *J. Aerosol Med.* **10**, 105–116. (doi:10.1089/jam.1997.10.105)
11. Morawska L, Johnson GR, Ristovski ZD, Hargreaves M, Mengersen K, Corbett S, Chao CY, Li Y, Katoshevski D. 2009 Size distribution and sites of origin of droplets expelled from the human respiratory tract during expiratory activities. *J. Aerosol Sci* **40**, 256–269. (doi:10.1016/j.jaerosci.2008.11.002)
12. Johnson GR *et al.* 2011 Modality of human expired aerosol size distributions. *J. Aerosol Sci* **42**, 839–851. (doi:10.1016/j.jaerosci.2011.07.009)
13. Vejerano EP, Marr LC. 2018 Physico-chemical characteristics of evaporating respiratory fluid droplets. *J. R. Soc. Interface* **15**, 1–10. (doi:10.1098/rsif.2017.0939)
14. Marr LC, Tang JW, Van Mullekom J, Lakdawala SS. 2019 Mechanistic insights into the effect of humidity on airborne influenza virus survival, transmission and incidence. *J. R. Soc. Interface* **16**, 20180298. (doi:10.1098/rsif.2018.0298)
15. Atkinson J, Chartier Y, Lúcia Pessoa-Silva C, Jensen P, Li Y, Seto WH. 2009 Natural Ventilation for Infection Control in Health-Care Settings - World Health Organization. Technical report.
16. Wang X, Chen C, Binder K, Kuhn U, Pöschl U, Su H, Cheng Y. 2017 Molecular dynamics simulation of the surface tension of aqueous sodium chloride: from dilute to highly supersaturated solutions and molten salt. *Atmos. Chem. Phys. Discuss.* **18**, 17 077–17 086. (doi:10.5194/acp-18-17077-2018)
17. Bourouiba L, Dehandschoewercker E, Bush JW. 2014 Violent expiratory events: on coughing and sneezing. *J. Fluid Mech.* **745**, 537–563. (doi:10.1017/jfm.2014.88)
18. Vuorinen V *et al.* 2020 Modelling aerosol transport and virus exposure with numerical simulations in relation to SARS-CoV-2 transmission by inhalation indoors. *Saf. Sci.* **130**, 104866. (doi:10.1016/j.ssci.2020.104866)
19. Samimy M, Lele SK. 1991 Motion of particles with inertia in a compressible free shear layer. *Phys. Fluids A* **3**, 1915–1923. (doi:10.1063/1.857921)
20. Milton DK. 2020 A Rosetta stone for understanding infectious drops and aerosols. *J. Pediatr. Infect. Dis. Soc.* **9**, 413–415. (doi:10.1093/jpids/piaa079)
21. Faeth G. 1983 Evaporation and combustion of sprays. *Prog. Energy Combust. Sci.* **9**, 1–76. (doi:10.1016/0360-1285(83)90005-9)
22. Schiller L, Naumann A. 1933 Über die grundlegende Berechnung bei der Schwerkraftaufbereitung. *Z. Ver. Dtsch. Ing.* **77**, 318–320.
23. Abramzon B, Sirignano W. 1989 Droplet vaporization model for spray combustion calculations. *Int. J. Heat Mass Transfer* **32**, 1605–1618. (doi:10.1016/0017-9310(89)90043-4)
24. Frössling N. 1938 Uber die verdunstung fallender tropfen. *Gerlands Beiträge zur Geophysik* **12**, 170–216.

25. Pruppacher H, Klett J. 1996 *Microphysics of clouds and precipitation*, 2nd edn. Berlin, Germany: Springer.
26. Dutcher CS, Wexler AS, Clegg SL. 2010 Surface tensions of inorganic multicomponent aqueous electrolyte solutions and melts. *J. Phys. Chem. A* **114**, 12 216–12 230. (doi:10.1021/jp105191z)
27. Fathi-Azarbayjani A, Jouyban A. 2015 Surface tension in human pathophysiology and its application as a medical diagnostic tool. *BioImpacts* **5**, 29–44. (doi:10.15171/bi.2015.06)
28. Mikhailov E, Vlasenko S, Niessner R, Pöschl U. 2003 Interaction of aerosol particles composed of protein and salts with water vapor: hygroscopic growth and microstructural rearrangement. *Atmos. Chem. Phys. Dis.* **3**, 4755–4832. (doi:10.5194/acpd-3-4755-2003)
29. Redrow J, Mao S, Celik I, Posada JA. 2011 Modeling the evaporation and dispersion of airborne sputum droplets expelled from a human cough. *Build. Environ.* **46**, 2042–2051. (doi:10.1016/j.buildenv.2011.04.011)
30. Gould JM, Weiser JN. 2001 Expression of C-reactive protein in the human respiratory tract. *Infect. Immun.* **69**, 1747–1754. (doi:10.1128/IAI.69.3.1747-1754.2001)
31. Effros RM, Hoagland KW, Bosbous M, Castillo D, Foss B, Dunning M, Gare M, Lin W, Sun F. 2002 Dilution of respiratory solutes in exhaled condensates. *Am. J. Respir. Crit. Care Med.* **165**, 663–669. (doi:10.1164/ajrccm.165.5.2101018)
32. Veldhuizen EJ, Haagsman HP. 2000 Role of pulmonary surfactant components in surface film formation and dynamics. *Biochim. Biophys. Acta Biomembranes* **1467**, 255–270. (doi:10.1016/S0005-2736(00)00256-X)
33. van Doremalen N *et al.* 2020 Aerosol and surface stability of SARS-CoV-2 as compared with SARS-CoV-1. *N. Engl. J. Med.* **382**, 1564–1567. (doi:10.1056/NEJMc2004973)
34. Jones TC *et al.* 2020 An analysis of SARS-CoV-2 viral load by patient age. *medRxiv (preprint)*.
35. Watanabe T, Bartrand TA, Weir MH, Omura T, Haas CN. 2010 Development of a dose-response model for SARS coronavirus. *Risk Anal.* **30**, 1129–1138. (doi:10.1111/j.1539-6924.2010.01427.x)
36. Gupta JK, Lin CH, Chen Q. 2010 Characterizing exhaled airflow from breathing and talking. *Indoor Air* **20**, 31–39. (doi:10.1111/j.1600-0668.2009.00623.x)
37. Gupta JK, Lin CH, Chen Q. 2009 Flow dynamics and characterization of a cough. *Indoor Air* **19**, 517–525. (doi:10.1111/j.1600-0668.2009.00619.x)
38. Pope SB. 2000 *Turbulent flows*. Cambridge, UK: Cambridge University Press.
39. Asadi S, Wexler AS, Cappa CD, Barreda S, Bouvier NM, Ristenpart WD. 2019 Aerosol emission and superemission during human speech increase with voice loudness. *Sci. Rep.* **9**, 1–10. (doi:10.1038/s41598-018-37186-2)
40. Bhagat RK, Davies Wykes MS, Dalziel SB, Linden PF. 2020 Effects of ventilation on the indoor spread of COVID-19. *J. Fluid Mech.* **903**, F1. (doi:10.1017/jfm.2020.720)
41. RAMP Task 7 Members. 2020 The ventilation of buildings and other mitigating measures for COVID-19: a focus on winter 2020. *The Royal Society Rapid Assistance for Modelling the Pandemic (RAMP) Project Task 7: Environmental and Aerosol transmission*, pp. 1–62. (https://arxiv.org/abs/2009.12781)
42. Chartered Institution of Building Services Engineers (CIBSE). 2015 Guide A: Environmental Design.
43. Government U. 2018 Classvent and Classcool school ventilation design tool. See http://www.gov.uk/government/publications/classvent-and-classcool-school-ventilation-design-tool.
44. de Oliveira PM, Sitte MP, Mastorakos E. 2020 tykyra: a model for viral decay in droplets/aerosol from respiratory releases. *GitHub*. (https://github.com/pdromo/tykyra)